Columnar grouping preserves synchronization in neuronal networks with distance-dependent time delays

Joseph S. Tumulty, Michael Royster,* and Luis Cruz†
Department of Physics, Drexel University, 3141 Chestnut Street, Philadelphia, Pennsylvania 19104, United States

(Received 4 June 2019; revised manuscript received 7 November 2019; accepted 10 January 2020; published 14 February 2020)

Neuronal connectivity at the cellular level in the cerebral cortex is far from random, with characteristics that point to a hierarchical design with intricately connected neuronal clusters. Here we investigate computationally the effects of varying neuronal cluster connectivity on network synchronization for two different spatial distributions of clusters: one where clusters are arranged in columns in a grid and the other where neurons from different clusters are spatially intermixed. We characterize each case by measuring the degree of neuronal spiking synchrony as a function of the number of connections per neuron and the degree of intercluster connectivity. We find that in both cases as the number of connections per neuron increases, there is an asynchronous to synchronous transition dependent only on intrinsic parameters of the biophysical model. We also observe in both cases that with very low intercluster connectivity clusters have independent firing dynamics yielding a low degree of synchrony. More importantly, we find that for a high number of connections per neuron but intermediate intercluster connectivity, the two spatial distributions of clusters differ in their response where the clusters in a grid have a higher degree of synchrony than the clusters that are intermixed.

DOI: 10.1103/PhysRevE.101.022408

I. INTRODUCTION

Structural organization of neurons is a characteristic that is observed throughout the brain and across different scales. For example, in the neocortical region of the mammalian brain, the degree of connectivity between functional areas is nonrandom, and has been found to exhibit small-world network characteristics [1–6]. These characteristics, in addition to being intrinsic, may be functionally important since deviations from nonrandom to more random network connectivities have been found to be correlated with neuropathology [7–9]. Not only at the macroscopic scale, but also at the cellular level neuronal networks have been found to form nonrandom structures [6,10–12]. This similarity in network properties at different scales suggests that basic underlying processes may operate across scales [13].

Recent work has shown that clusters of several neurons are synaptically connected and may be engaged in basic computational function [12,14–16]. Interestingly, these nonrandom structures have been seen to spontaneously form *in vitro* [17], suggesting that this is an intrinsic mechanism. At a comparatively larger scale, but still at a submillimeter scale, structures have been found where hierarchical connections form networks of clusters [18–23]. Groups of nodes inside these clusters or modules preferentially link to other nodes in the same community while being sparsely connected to the rest of the network [24]. It is found that these networks are robust to shuffling of connections [25], while sparser connections between modules enable efficient intermodule integration of information [26] and high within-module connection density promotes communication efficiency [27].

Variations in connectivity result in different distances between connected neurons that in turn yield different delay times between action potentials and their postsynaptic signals. Varying delay times directly affect synchronization [28–30], and distance-dependent time delays connect network structure with dynamics [31,32]. Because clustering and function may be correlated, here we investigate whether clustering offers any advantage to the firing dynamics of a network. Previous computational work showed that a network with hierarchical modular connectivity, but without distance dependence, expands the phase space of spontaneous activity [20]. Time delays always disrupted synchronization in all-connected networks [31], while in a distance-dependent delay model with variable connectivity but without explicit clustering, the most synchronized network was found to be the one with intermediary connectivity between long range and nearest neighbor [32]. In more recent computational work, tuning connection strength parameters or the number of inhibitory neurons in a clustered neuronal network with fixed intercluster connectivity modulated the level of synchronization of the network [33].

To specifically determine how clustering affects dynamics, here we consider a three-dimensional (3D) connected network, built from a stochastic block model [34], with clusters of tunable neuronal connectivity and distance-dependent signal delay times. We assign neurons to different clusters, referred to here as groups, and construct two types of networks: one in which different groups are placed in a grid pattern, and the other where neurons from different groups are spatially intermixed. We use two independent variables in this comparison: the degree of connectivity per neuron and the degree of intergroup connectivity. We measure the performance of and

*physicalreview@michaelroyster.org
†Corresponding author: ccruz@drexel.edu

gauge the differences between these networks by measuring the degree of synchrony in their firing dynamics. Network firing synchronization is important as, for example, it can be an indicator of attention [35], response to visual stimuli [36], and to an increase in information transfer efficiency [37]. On the other hand, a high degree of synchronization may be related to the onset of seizures in humans with epilepsy, as shown in the case of local hypersynchronization [38]. The measure of synchronization that we use here quantifies different degrees of spiking synchrony. Our results suggest that networks with neurons connected in a grid have a higher degree of synchrony than randomly connected networks for a large range of inter- and intracluster connectivity values examined here.

II. METHODS

To construct the neuronal networks, we assign random 3D positions to neurons inside a cube and assign these neurons to groups (clusters) that are either spatially separated or mixed. We then connect the neurons according to rules that differentiate between neurons within their own group and across different groups. Lastly, we perform firing simulations where action potentials are explicitly generated. We obtain measurements of the spiking synchrony as a function of two independent variables: the average neuronal connectivity and the degree of connectivity between groups. This process is detailed below.

A. Neuronal placement, grouping, and connections

For each network, we generate a set of random neuronal positions contained within a 3D box of side length L_b. We then label neurons with a group ID according to two different methods. In the first method, we overlay an $n \times n$ grid onto the xy coordinates of the network and label each neuron with a group ID that corresponds to the quadrant in which their xy coordinates fall, as shown for a 2×2 case in Fig. 1(a). In the second method, we randomly assign neurons to group IDs, as shown in Fig. 1(b). We refer to these grouping methods as grid and mixed grouping, respectively. To control for variability when comparing data from the two grouping methods we generate two networks, each using one of the two different grouping methods, but both using the same number of neurons, spatial positions, number of groups, and number of neurons per group.

Once the neurons are placed and grouped, we connect neurons according to one of two possible schemes depending on whether they are excitatory or inhibitory neurons. In the first scheme excitatory neurons are connected to other neurons with either an intra- or intergroup connection probability. We modulate this by using a continuous bias parameter, δ, with value in the 0–1 range where 0 gives equal probability to all connections independent of group, and 1 means that all connections are intragroup connections (no connection between different groups). The other important variable is the average number of outgoing connections per excitatory neuron m. All of our results are expressed in terms of these two independent parameters, m and δ. They have different overall effects: while increasing m creates a more densely connected

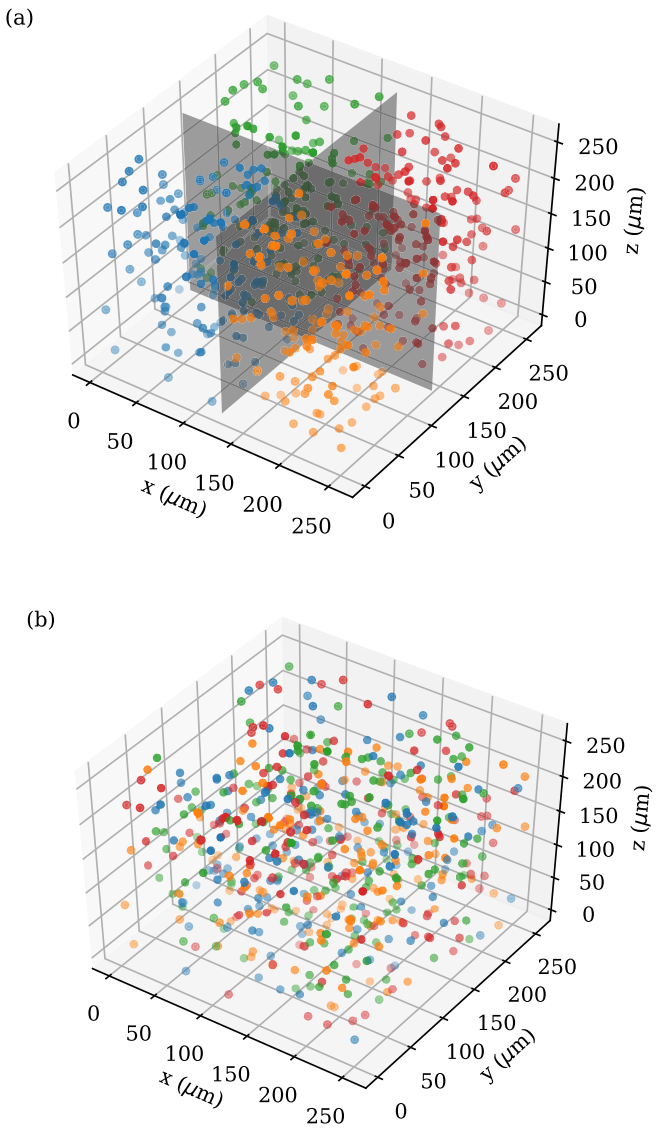

FIG. 1. Neuronal placement for the grid and mixed grouping. (a) A grid grouping network where a 2×2 grid in the xy plane separates neurons into four different groups based on their xy positions. (b) A mixed grouping network where neurons belong to randomly assigned groups. The four different colors indicate the four different groups.

network, increasing δ makes networks with increasingly isolated groups.

In any given network we assign neurons an average m and δ, which results in a symmetric connection probability matrix $\mathbf{P}$. Thus, the probability of having a connection between neurons i and j, belonging to groups G_i and G_j, respectively, is

$$\mathbf{P}_{ij} = \begin{cases} 0 & i = j \\ p_{\text{inter}} + p_{\text{intra}} & G_i = G_j, \\ p_{\text{inter}} & \text{otherwise} \end{cases} \tag{1}$$

where

$$p_{\text{inter}} = \frac{m(1-\delta)}{N-1}$$
$$p_{\text{intra}} = \frac{m\delta}{M^{(G_i)}-1}. \tag{2}$$

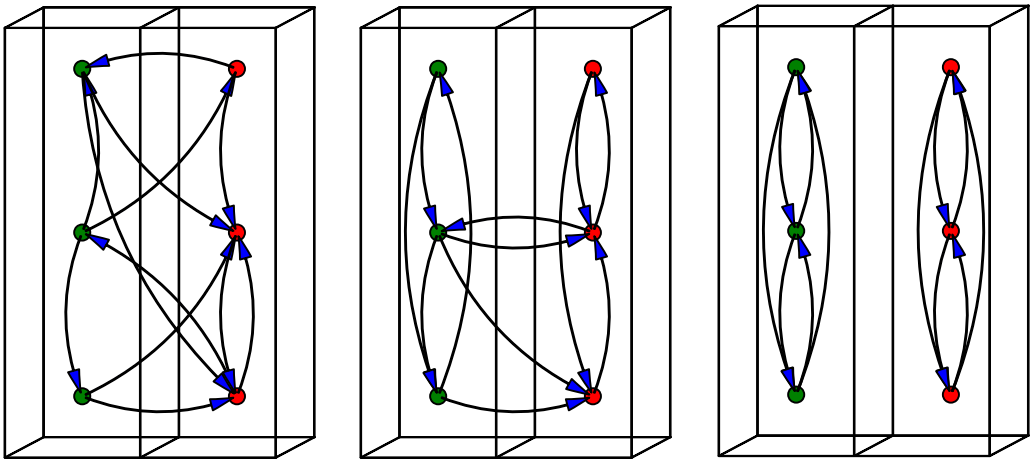

FIG. 2. Illustration of the different connections between two groups as a function of δ (with outgoing number of connections per neuron $m = 2$): (a) $\delta = 0$ with completely random connections, (b) $\delta = 0.5$ giving bias towards intragroup connections, and (c) $\delta = 1$ with completely independent groups.

N is the number of neurons in the system, and $M^{(G_i)}$ is the number of neurons in the ith group. When $\delta = 0$, we recover a uniform random distribution of connections and when $\delta = 1$, all connections are within groups (see Fig. 2). The probabilities in Eq. (2) satisfy the constraint

$$m = (N-1)p_{\text{inter}} + (M^{(G_i)} - 1)p_{\text{intra}} \tag{3}$$

independent of δ except in the case of saturation. Saturation occurs when the desired number of intragroup connections $m^{(i)}_{\text{group}}$ is greater than the total number of possible connections within the group $M^{(G_i)} - 1$. Modifying (3) shows that the expected value of $m^{(i)}_{\text{group}}$ is

$$\langle m_{\text{group}} \rangle = m\left[\left(1 - \frac{\langle M \rangle - 1}{N-1}\right)\delta + \frac{\langle M \rangle - 1}{N-1}\right], \tag{4}$$

where

$$\langle M \rangle = \frac{N}{\text{number of groups}}. \tag{5}$$

The maximum m that we can use without saturation for all values of δ is then

$$m = \langle M \rangle - 1. \tag{6}$$

Because all connections end at another neuron in the system, the average number of incoming connections per neuron is also equal to m.

Connections are simply created by first assigning a random value to each possible connection and then forming the connection only if the random value is less than the probability. The resultant distribution of actual connections per neuron in a connected network then follows a normal distribution, with the majority of neurons having a number of outgoing connections close to the average, and a minority having few or many outgoing connections (hubs). Example distributions of the number of connections are provided in Fig. S1 in the Supplemental Material [39].

When constructing networks that include inhibitory neurons, we use the above method for all outgoing excitatory connections, but we connect the inhibitory neurons to all other neurons (independent of groups) based on a distance-dependent, exponentially decaying probability [40] given by

$$P_{ij} = e^{-d_{ij}/D}. \tag{7}$$

The parameter D, a decay distance, is determined by fixing the number of outgoing connections per inhibitory neuron, m_{I}, such that D is the numerical solution to

$$m_{\text{I}} = \frac{\sum_{i \neq j} e^{-d_{ij}/D}}{N_{\text{I}}}, \tag{8}$$

where d_{ij} is the Euclidian distance between the ith inhibitory neuron and any other neuron j, and N_{I} is the number of inhibitory neurons in the network. Note that m_{I} is a parameter independent of m, which is a variable under investigation in this work. This process still renders an average m for excitatory neurons and m_{I} for inhibitory neurons.

An important outcome of these probability distributions is that most of our networks can be characterized as small-world networks. A small-world network, as defined by Watts and Strogatz, is one that, compared to random networks, has a higher degree of clustering while still maintaining an equivalent average path length (good global connectivity quantified in number of hops, not Euclidian distance) between any two neurons [41]. To show this result, we calculate the Watts-Strogatz clustering coefficient, a measure of the fraction of neurons connected to any one neuron that are also connected to each other [41]. We do this for our networks and corresponding random networks of the same number of nodes and edges per node. We determine average path length by searching for the shortest path (in number of hops) between all pairs of neurons and averaging these paths over the network. Figure 3 shows that with increasing δ, the relative clustering coefficient, γ, increases while the average path length, λ, stays approximately equal to that of a random network, only

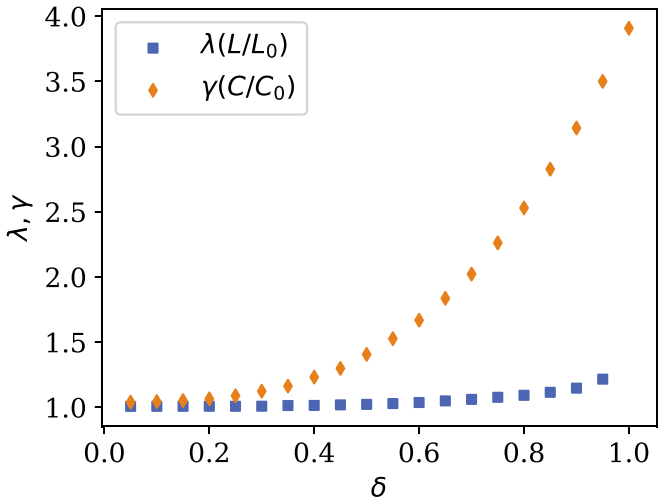

FIG. 3. Plot showing relative clustering ($\gamma = C/C_0$) and relative average path length ($\lambda = L/L_0$) as a function of δ. C, and L are the Watts-Strogatz clustering coefficient and average path length, respectively, for a connected network based on the probability distributions described in Eq. (2) while C_0 and L_0 are the corresponding values for a random network of equal size (same number of nodes and directed edges). Each data point represents an average value over 10 systems for each specified value of δ (there is little dependence on m, thus only $m = 25$ is plotted). The small-worldness of a network can be quantified as the ratio of relative clustering to relative average path length (γ/λ).

increasing slightly at very high δ (at $\delta = 1$ there are pairs of neurons with no possible paths between them yielding infinite path lengths). Thus, the ratio γ/λ, a measure of the degree to which a network is a small-world network, is greater than 1 for systems with $\delta > 0.2$ and all values of m indicating that most of our networks can be characterized as small-world networks.

To avoid edge effects inherent when using any finite-sized network, for all networks we consider neuron connection lengths (Euclidian distance) according to their minimum image distance. That is, having chosen two neurons to be connected, we assign the distance between them to be the minimum of: (i) their direct distance as measured using coordinates within the box or (ii) the distance between one of the neurons and the other neuron in an equivalent image of the network.

B. Neuron model and firing dynamics

To simulate the firing of the neurons in our networks, we use the package NEURON [42] to model the membrane potential using a Hodgkin-Huxley mechanism. We model the neurons using a single compartment with sodium, potassium, and leaky ion currents. The specific parameters used for the models of our pyramidal cortical neurons and inhibitory interneurons are taken from Destexhe *et al.* [43] and McCormick *et al.* [44] (see Table SI [39]). The model uses an equation for the membrane potential that depends on intrinsic ionic currents and synaptic currents,

$$c_m \frac{dV}{dt} = -i_{\text{int}} - i_{\text{syn}}. \tag{9}$$

The intrinsic ionic currents (i_{int}) are made up of sodium (i_{Na}), potassium (i_{K}), and leaky currents (i_L), each with their own respective conductance, g, and reversal potential, E. In this model the pyramidal neurons include an extra potassium current (i_M) that helps to regulate firing frequency [44]. As the sodium and potassium channels are voltage gated, their conductances are a function of voltage-dependent activation and inactivation variables [$n(V)$, $m(V)$, $h(V)$] and a maximum conductance $\bar{g}$. Each current is then calculated as the product of the varying conductance and the membrane potential relative to their reversal potential,

$$\begin{aligned} i_{\text{int}} = {} & \bar{g}_{\text{Na}} m(V)^3 h(V)(V - E_{\text{Na}}) + \bar{g}_{\text{K}} n_K(V)^4 (V - E_{\text{K}}) \\ & + \bar{g}_M n_M(V)(V - E_{\text{K}}) + g_L(V - E_L). \end{aligned} \tag{10}$$

Each activation and inactivation variable obeys its own differential equation that is a function of membrane potential of the form:

$$\begin{aligned} \frac{dn}{dt} &= \frac{n_\infty(V) - n}{\tau_n(V)} \\ \frac{dm}{dt} &= \frac{m_\infty(V) - m}{\tau_m(V)} \\ \frac{dh}{dt} &= \frac{h_\infty(V) - h}{\tau_h(V)}. \end{aligned} \tag{11}$$

More details on the components ($n_\infty, m_\infty, h_\infty, \tau_n, \tau_m, \tau_h$) of the activation/inactivation variables can be found in Sec. I of the Supplemental Material [39]. The values of the parameters that we use in the model are listed in Table SI.

Once the ith neuron's membrane potential rises above a threshold of 10 mV, an evoked action potential (AP), or spike, is transmitted to each connected neuron j ($0 < j \leqslant m$). These spikes result in postsynaptic currents at the target neuron, i_{syn}, whose conductances depend on the type of connection. More specifically, the synaptic conductance depends on whether the source and target neurons are excitatory (E) or inhibitory (I) according to:

$$\begin{aligned} \text{E} \to \text{E} \quad & g_{\text{syn}} = +0.45\mu\text{S} \\ \text{E} \to \text{I} \quad & g_{\text{syn}} = +0.20\mu\text{S} \\ \text{I} \to \text{E} \quad & g_{\text{syn}} = -0.05\mu\text{S} \\ \text{I} \to \text{I} \quad & g_{\text{syn}} = -0.10\mu\text{S}. \end{aligned}$$

Because our neuronal networks model only a small population of neurons in the brain, we model external neuronal chatter originating at farther distances as spikes drawn from a Poisson distribution with an average stimulation interval of 35 ms. These series of spikes are independent for each neuron and are the only driving stimulation in each network that persists throughout the length of the simulations. Each driving spike also contributes to the total synaptic current, i_{syn}, with conductance $g_{\text{syn}} = 1\ \mu S$. For all synaptic currents, the conductances decay exponentially obeying

$$\frac{dg_{\text{syn}}}{dt} = -g_{\text{syn}}/\tau,$$

where $\tau = 1$ ms.

To model distance-dependent signal delays, each evoked spike arrives at the target neuron after a delay time given by

$$t_{ij} = d_{ij}/v,$$

where v is the propagation speed of the signals and d_{ij} is the Euclidian distance between the source and target neurons. We model the neuronal spacing and density using values previously used for layer III of the prefrontal cortex in rhesus monkey brains [45].

C. Measures of spike synchrony

For each neuron, we record the times at which they generate spikes and construct a spike train. In our model, spike trains are in general nonperiodic and may contain regions of high and/or low frequency of spikes. We measure synchrony between two spike trains by measuring the distance between them, thus the larger the distance, the more dissimilar two spike trains are. Typical approaches to calculate this quantity include the Victor-Purpura and van Rossum distances [46–48] that are time-scale dependent. An alternative measure, and the one used here, is the SPIKE-distance method proposed by Kreuz *et al.* [49,50]. This method is more appropriate to our case since it is a parameter-free and timescale-independent measure of spike train synchrony that dynamically adapts to the timescale of the spike trains. The SPIKE distance is bounded on the interval [0, 1], where 0 indicates identical spike trains and 1 indicates maximally asynchronous, dissimilar spike trains.

To define the bivariate SPIKE distance [49,50], consider spike trains of two neurons with labels $n = 1, 2$. At any time t, let $\Delta t_P^{(n)}(t)$ be the time between the previous spike of neuron n and the other neuron, $\Delta t_F^{(n)}(t)$ be the time between the following spike of neuron n and the nearest spike of the other neuron, $x_P^{(n)}(t)$ and $x_F^{(n)}(t)$ be the times to the previous and following spikes of neuron n, respectively, and $x_{\mathrm{ISI}}^{(n)}(t)$ be the total interspike interval (ISI) between previous and following spikes of neuron n ($x_{\mathrm{ISI}} = x_P + x_F$) (see Sec. II in the Supplemental Material [39] for formal definitions). Having these quantities, we can then calculate the local weighted spike time difference, $S_n(t)$, for each neuron (the weighting makes it such that spike time differences closer to the time, t, have a greater contribution),

$$S_n(t) = \frac{\Delta t_P^{(n)}(t) x_F^{(n)}(t) + \Delta t_F^{(n)}(t) x_P^{(n)}(t)}{x_{\mathrm{ISI}}^{(n)}(t)}. \tag{12}$$

We can then calculate the dissimilarity profile, $S(t)$, by weighting the contributions from each neuron's $S_n(t)$ value by the neuron's interspike interval (ISI) at time t. This weighting helps account for differences in firing frequency,

$$S(t) = \frac{S_1(t) x_{\mathrm{ISI}}^{(2)}(t) + S_2(t) x_{\mathrm{ISI}}^{(1)}(t)}{2\langle x_{\mathrm{ISI}}^{(n)}(t)\rangle_n^2}. \tag{13}$$

Finally, we obtain a single value for the distance between the pair of spike trains by simply calculating the average value of this profile, $S(t)$, over the whole simulation time of length T. This is what is called the SPIKE distance for the two neurons under consideration,

$$D_S = \frac{1}{T}\int_{t=0}^{T} S(t)dt. \tag{14}$$

We obtain the average SPIKE distance for any one network simulation by calculating the average of the SPIKE distance using every pair of neurons in the network.

Because this measure relies on the distance between spike times from a pair of neurons, it gives a measure of simultaneity of spike events over a whole train of spikes. Thus it corresponds most closely to a measure of event synchronization.

D. Parameters and statistics

The size of the 3D box containing each neuronal network is $L_b = 256$ μm. Using neuron size and density parameters from previous work [45], we generate 10 systems with only excitatory neurons and 10 with additional inhibitory neurons where all neuronal spatial locations are chosen at random. We use each set of positions for both a grid and mixed grouping connected network. The networks contain on average $N_E = 571$ excitatory neurons and in networks that include inhibitory neurons, we add on average $N_I = 139$ inhibitory neurons (lowering the average N_E to 556 corresponding to $\approx$20% inhibitory neurons). We carry out simulations with total time lengths each of 10000 ms and record the times of spikes. To avoid transient behavior we discard the first 500 ms of simulation time. We sample the $[m, \delta]$ phase space for different values of m and δ in the range of $m = [1, 45]$ and $\delta = [0, 1)$. The upper limit of the m range guarantees that our networks are well below the saturation point discussed in Sec. II A for networks with smaller groups (nine groups lead to saturation point $m \approx 60$). For the networks with inhibitory neurons, we test different values for m_{I} from $m_{\mathrm{I}} = 10,\ 35,\ 45$ in Eq. (8). We select values of m and δ at random, except in regions with higher values of m where more phase points are sampled. We explored a large range of propagation speeds and display results here for only $v = 7.5$ μm/ms, which most accentuates the features of interest. With this propagation speed and the connection lengths in our networks the resulting delay times between neurons range from 1 ms to about 30 ms.

III. RESULTS

A. Networks of excitatory neurons

After a transient period, less connected systems (low m) enter a state of noisy activity, as exemplified in Fig. 4(a), while more highly connected systems (high m) synchronize in networkwide coordinated events, as illustrated in Fig. 4(b). Figure 5 shows heat map representations of the phase space of SPIKE-distance data showing the degree of synchrony for four group networks (2×2 grid vs four mixed groups). The scale in the figure ranges from red (asynchronous; SPIKE distance = 0.28) to blue (synchronous; SPIKE distance = 0.12). The SPIKE-distance value associated with the red region of the diagrams ($\approx$0.28) is the same as the value obtained in an equivalent network with totally unconnected independent neurons; therefore this value corresponds to maximum asynchrony given our simulation parameters. This maximum value measured in our networks is much smaller than the

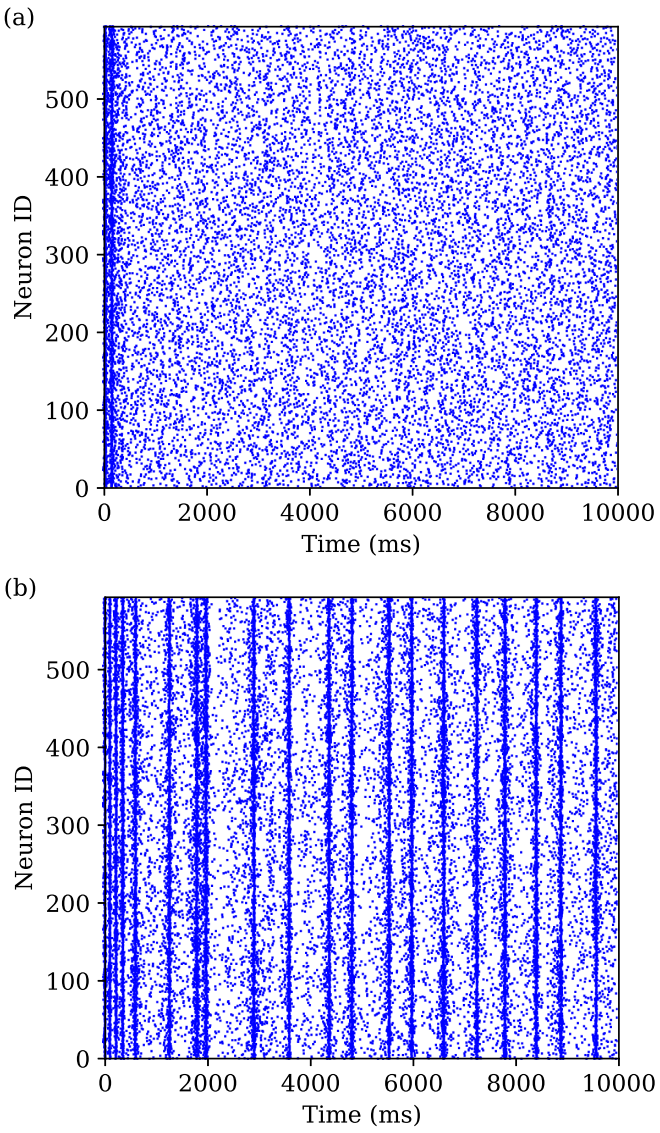

FIG. 4. Example raster plots of neuronal spikes as a function of simulation time for all neurons in two networks with $\delta = 0.5$ and two different number of connections per neuron: (a) $m = 20.2$ and (b) $m = 35.5$.

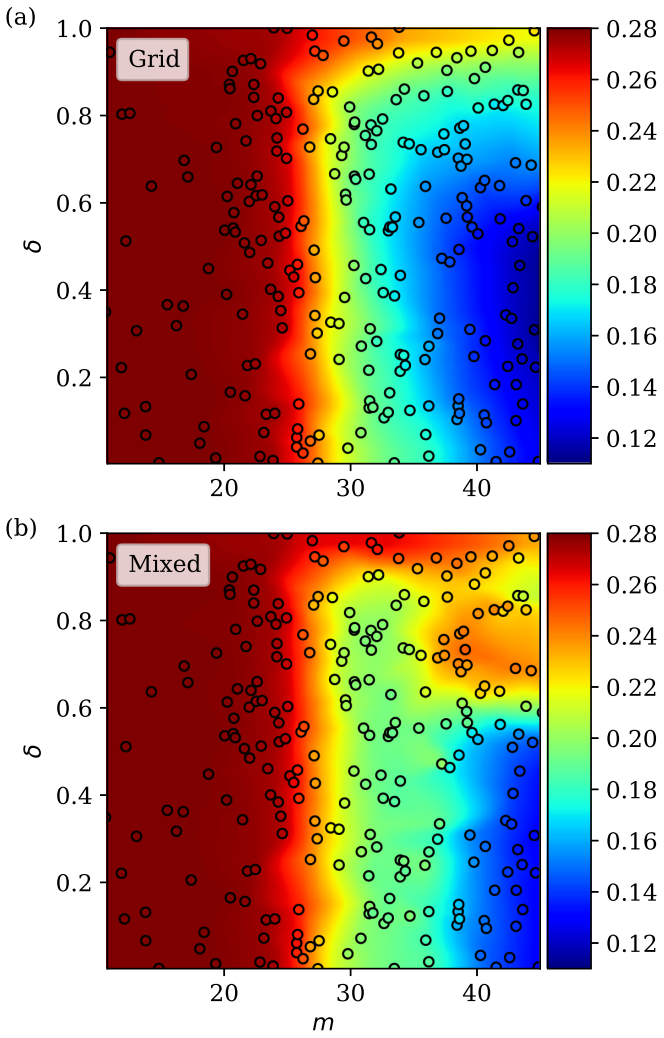

FIG. 5. Phase space diagrams of the average SPIKE distance for the (a) 2×2 grid and (b) mixed groupings as a function of m and δ. Sampled m, δ points are represented by open circles and their values are averages over 10 networks. The underlying color map is linearly interpolated from these data. The color scale is in units of the SPIKE-distance metric, which ranges from 0–1.

theoretically maximum value of the instantaneous SPIKE distance between a pair of neurons (see Fig. S2 [39] for an illustration).

Both sets of data shown in Fig. 5 indicate a rather sharp reduction in SPIKE distance (from red to blue) at a parameter-dependent $m' \approx 25$ (see Fig. 6) that occurs simply because as the number of connections (and thus current) increases [e.g., starting from Fig. 4(a)], at $m \geqslant m'$ any fluctuation will provoke repeated cascades of firings [e.g., Fig. 4(b)], indicative of a synchronous state. The location of this transition can be estimated by using an effective firing rate of neurons, x, and m. On average, a neuron receives n firings per unit time that can be approximated as $n = mx(1 + m/n_c)$, where the first term is an effective rate of input spikes arising from all m connections, and the second term is due to firings from the neighbors of the connected neurons (proportional to m and inversely proportional to the minimum number of inputs necessary to trigger a spike, n_c). At the transition $n = n_c$ and $m = m'$. From our data on systems close to the transition, we directly measure that in a given 10 ms interval, about five excitatory inputs are needed to trigger a spike ($n_c \simeq 5$) and the average firing rate $x = 0.03$ (3 Hz). Solving for m' we obtain a value $m' = 26.5$, in agreement with the transition value observed in Fig. 6.

The transition in SPIKE distance is reflected in the firing dynamics in these two regimes as shown in the raster plots from each region that show a clear asynchronous to synchronous transition (Figs. S3 and S4 [39]). The change between these two regimes corresponds to a transition between two fundamentally different dynamical states of the networks. We show this by performing an independent calculation of the histogram of sizes of networkwide firing events (Fig. S5) in which events are defined as spikes occurring within a small window of time, and the size of the event is the number of spikes in that window. When plotting the number of events of

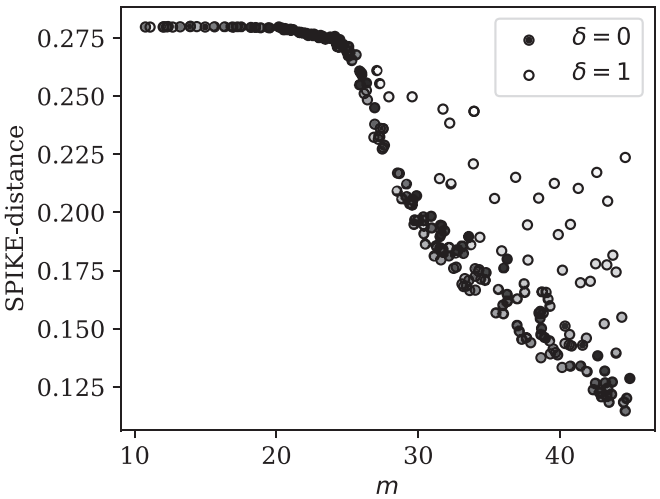

FIG. 6. Dependence of average SPIKE distance on connections per neuron for the grid grouping network, highlighting the sharp drop of the average SPIKE distance. Different values of the bias parameter, δ, are represented by varying shades of gray.

a certain size vs the size of the events we find that networks in the asynchronous regime exhibit a peaked distribution at small event sizes while in the synchronous region networks exhibit a power-law behavior [Fig. S5(a)], an indication of correlations [51]. Further, when doing a linear fit of the log-log plot of all such histograms throughout the entire phase space [Fig. S5(b)] we find that the regression residuals exhibit a sharp decrease at a similar m value as in Fig. 6.

Another feature shown in Fig. 5 that is common to both the grid and mixed groupings is a narrow horizontal asynchronous region above $\delta = 0.9$ for all values of m. This is because at high δ the groups are nearly completely unconnected from each other and the local firing patterns, even when synchronized, are not synchronized across groups. Thus, the globally averaged SPIKE distance will not yield a value corresponding to synchronous behavior.

By far the most important feature in this figure, and the main focus of this paper, is the clear difference between the two groupings at high m and δ (top-right corner). In this region of the phase space, the mixed grouping appears asynchronous while the grid grouping does not (see individual raster plots shown in Figs. S3 and S4 with $m = 39.14$ and $\delta = 0.73$). By calculating the histogram of sizes of firing events we observe that while in this region the grid grouping follows power-law behavior (synchronous), the corresponding histogram for the mixed grouping shows a peaked distribution (asynchronous) at the place where they differ the most (Fig. S6).

B. Statistical significance of the difference in SPIKE distance between grouping systems

To determine whether the differences between the two phase space diagrams in Fig. 5 are statistically significant, we first subtract both phase diagrams [Fig. 7(a)] and then plot [Fig. 7(b)] the region $m = [37, 45]$, $\delta = [0.65, 0.75]$ containing the largest SPIKE-distance differences found in Fig. 7(a).

By comparing both sets of data from Fig. 7(b) we can see that the size of the difference in the region of interest ($\approx$0.08)

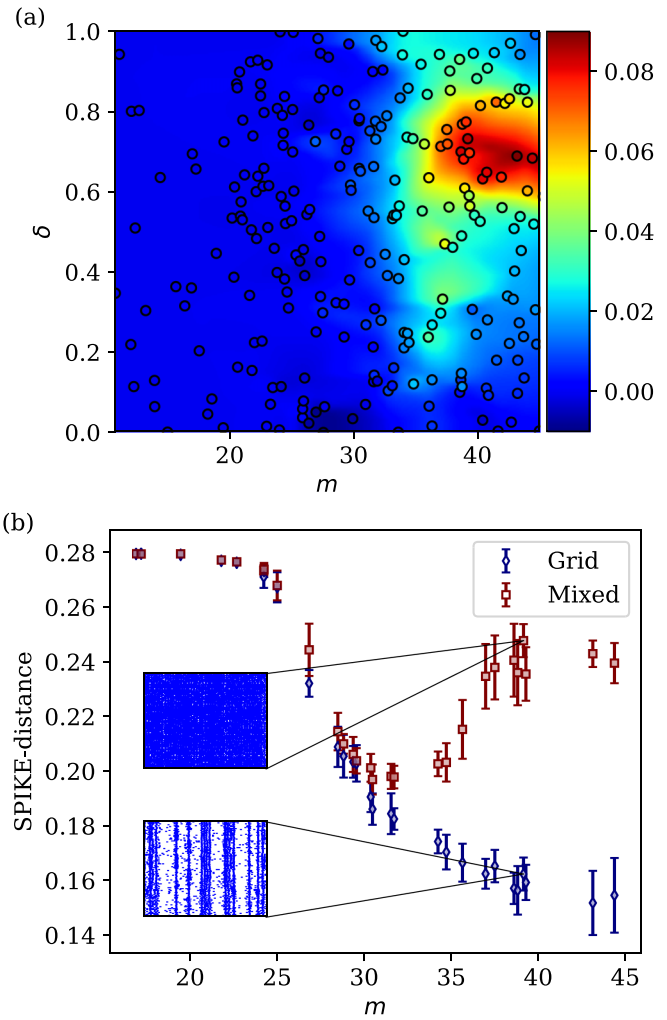

FIG. 7. (a) Difference in the SPIKE-distance data of Fig. 5 (mixed grid). Color scale is in units of SPIKE distance. (b) Dependence of the average SPIKE distance on m, for a range of δ between 0.65 and 0.75 (error bars show 1 standard deviation of the mean). Insets show raster plots of spikes for 100 neurons spanning 5 s of simulation time.

is much larger than the standard deviations of the means of each set (on the order of 0.01), thus statistically significant. Therefore in this region grid grouping is significantly more synchronized than the mixed grouping. A reason for this difference is shown in the raster plot for the mixed grouping that shows continuous network activity clearly exhibiting a hyperactive state leading to the higher value of the SPIKE distance. We also show in the Supplemental Material (see Sec. III of the Supplemental Material and Fig. S7 [39]) that when we split the network into smaller groups (3×3 grid), the difference between mixed and grid grouping is preserved.

C. δ dependence

To understand the origin of the enhanced synchronization in the region of interest resulting from grid grouping, we investigate structural properties that could play a role in the dynamics. Because the average path length (number of hops)

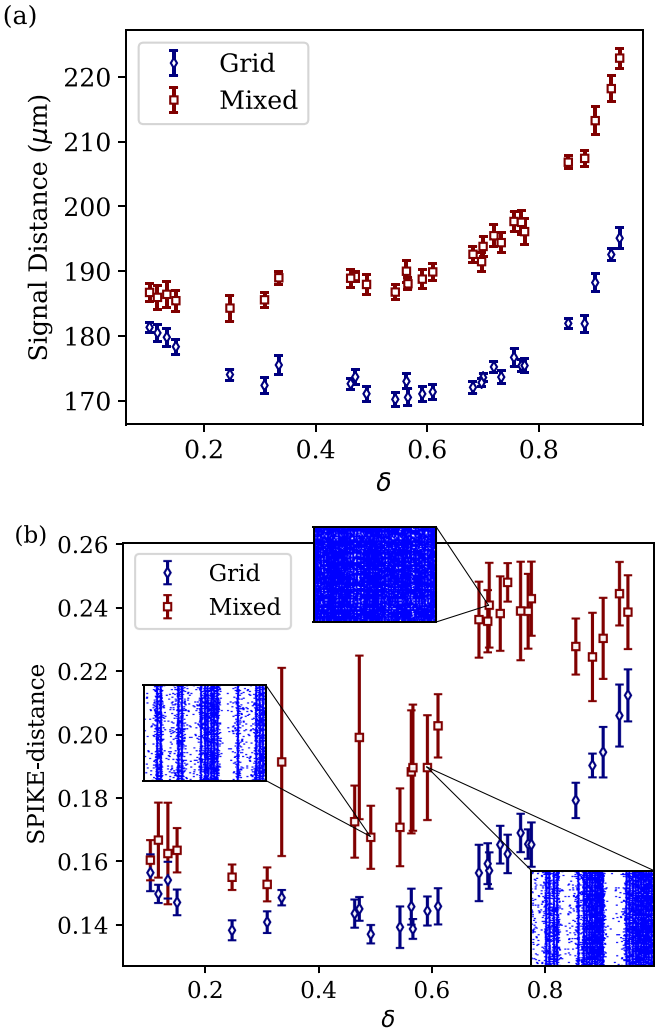

FIG. 8. δ dependence of (a) the average signal distance between pairs of neurons and (b) the average SPIKE distance for $m = [37, 40]$. Insets in (b) show raster plots of spikes for 100 neurons spanning 5 s of simulation time.

between two neurons is insensitive to δ (Fig. 3), we instead consider the signal distance. We define the signal distance between two neurons as the sum of the physical lengths of each intermediary connection along the shortest path between those neurons [52]. Figure 8(a) shows the average signal distance as a function of δ in the range of $m = [37, 40]$. First, this figure shows that for networks with grid grouping, as δ initially increases from 0, the signal distance slightly decreases. This is because increasing δ decreases the number of intergroup connections that are mostly long-range connections in grid networks. Second, at intermediate values of δ, the average signal distance, a property that is related to the effective accessible volume to neurons in a group, is lower in the grid grouping compared to the mixed grouping because the accessible volume is smaller than the entire box (unlike in the mixed grouping, as $\delta \to 1$ the grid grouping volume goes to one-quarter of the total volume). Third, for both types of grouping, as δ increases beyond approximately $\delta > 0.6$, the average signal distance starts to increase instead. This is because, for these values of δ, there is a greatly reduced number of intergroup connections resulting in a reduced number of neurons that bridge different groups. This means that signal distances will increase as all of the paths connecting different groups will have to cross using the remaining bridge neurons making the distances, on average, longer.

With this quantity in hand, we can now examine the δ dependence in the $m > 35$ region, shown in Fig. 8(b). The SPIKE distance is observed, for the grid grouping, to first slightly decrease for $0 < \delta < 0.2$, level out for $0.4 < \delta < 0.6$, and finally sharply increase for $\delta > 0.6$. On comparing Figs. 8(a) and 8(b) for the grid grouping, it is clear that the SPIKE distance is proportional to the signal distance. Thus, shorter physical distances in the grid grouping improve the chance of obtaining synchronized firing dynamics, which is consistent with shorter propagation times of signals.

Looking now at the mixed grouping, the previous rationale using signal distance does not explain the hyperactive state with an increase in SPIKE distance in the $\delta = [0.65, 0.75]$ region shown in Fig. 8(b). For this we need to look not at structural properties, but to dynamics. Raster plots from this region indicate that contrary to the grid, the hyperactive state in the mixed grouping exhibits almost continuous spikes [Figs. 7(b), S3, and S4]. In a typical synchronous state, raster plots show pronounced activity followed by gaps as shown in Fig. 4(b). Part of the reason for these gaps is the large number of neurons in their refractory period preventing subsequent firing [see Fig. S8(a)]. In contrast, raster plots in the hyperactive state indicate that there is a constant supply of ready-to-fire neurons throughout the network [Fig. S8(b)]. This suggests that there are different subgroups of neurons that take turns on firing together, but that by cascading their spikes, the global network lacks synchrony as defined by the SPIKE distance.

D. Effect of inhibitory neurons

To increase the level of realism of the model, we add inhibitory neurons to the networks as outlined in Sec. II. Different values for the connections per inhibitory neuron $m_{\mathrm{I}} = 10$, 35, 45 were explored having only the effect of shifting the m value of the transition toward higher values in the phase space. Figure 9 shows the SPIKE-distance phase space diagrams for both grouping methods using $m_{\mathrm{I}} = 10$.

From the figure, one effect of inhibitory neurons is to increase the overall values of the SPIKE distance as compared to Fig. 5. It also shifts the point at which the asynchronous to synchronous transition occurs that we can estimate from the figure to be about $m'' \approx 32$. This shift can be understood in terms of the effect of the number of connections on the postsynaptic current of excitatory neurons. As a reference, the maximum change in conductance in the purely excitatory system is given by $m' \times g_{EE}$, where m' is the threshold number of connections ($m' \approx 25$; from Fig. 5) and $g_{EE} = 0.45\ \mu S$. If we assume that, with inhibitory neurons, the same change in postsynaptic current should occur, then $(0.8 \times m'' \times g_{EE}) + (0.8 \times m_{\mathrm{I}} \times g_{IE}) = (m' \times g_{EE})$ (with 80% of connections terminating at an excitatory neuron, and $g_{IE} = -0.05\ \mu S$). Solving for the new threshold number of connections gives $m'' \simeq 32.4$, corresponding to the estimated value above.

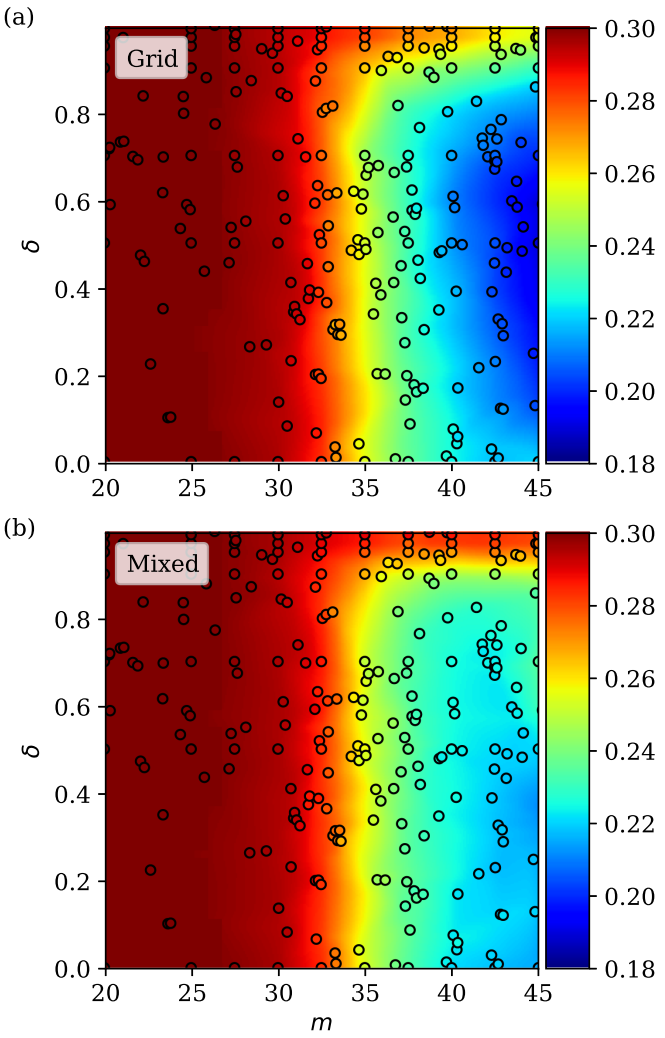

FIG. 9. Phase space diagrams of the average SPIKE distance for the (a) 2×2 grid and (b) mixed groupings with 20% inhibitory neurons as a function of m and δ. Sampled m, δ points are represented by open circles and their values are averages over 10 networks. The underlying colormap is linearly interpolated from these data. The color scale is in units of the SPIKE-distance metric.

Additionally, a visual comparison of Figs. 9(a) and 9(b) suggests that the difference between the two groupings is less than that observed in the purely excitatory networks. However, the quantitative difference is still significant, as can be seen in Fig. 10 for $m > 40$. The present reduction in the difference between the grid and mixed grouping schemes can be understood structurally by considering the following: because inhibitory neurons are connected independently of grouping, these additional connections generally increase intergroup communication and reduce the structural differences between grid and mixed groups. Dynamically, inhibitory neurons prevent the mixed system from entering the hyperactive state seen in Fig. 7; however, the raster plots still indicate a high level of activity in the same region of the phase space (see inset in Fig. 10). It is this highly active state that still causes the synchronization performance of the mixed grouping to be decreased.

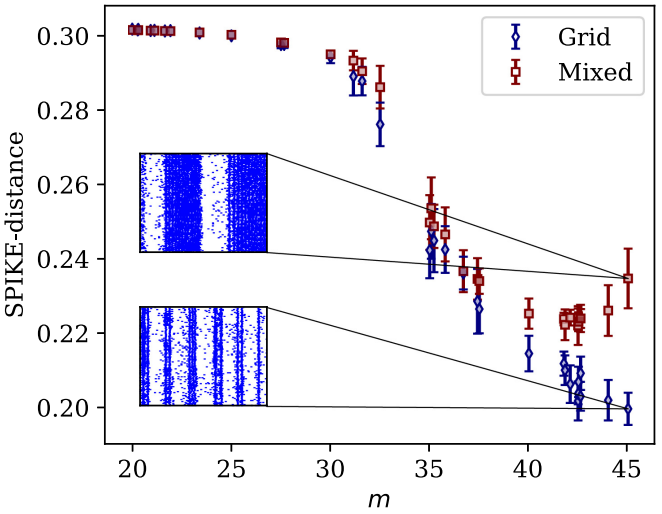

FIG. 10. Dependence of the average SPIKE distance on m, for a range of δ from 0.65–0.75 for networks with 20% inhibitory neurons. Insets show raster plots for 100 excitatory neurons spanning 5 s of simulation.

IV. DISCUSSION

In this work, we study the effects of structure and connectivity on the firing dynamics of a network of grouped neurons that may be important in cortical neuronal networks [15]. For this, we connect clusters of spatially segregated interconnected neurons similar to those observed in different connectomes in nature [53] (grid grouping) and compare their firing dynamics to a control case (mixed grouping). We find that although grouped and mixed networks have a very similar phase space, there is a region where grid grouping has a higher degree of synchrony. This result is preserved when we shrink the size of the groups as well as when including inhibitory neurons in our model.

To find the origin of this phenomena, we analyzed the average signal distances for each of the two groups and found significant differences. However, we also found that the average signal distances also differ in regions where both phase diagrams coincide, thus this quantity does not fully explain the disparity in synchrony. It is when we look at the corresponding raster plots that we find that contrary to grid grouping, mixed grouping is susceptible to hyperexcitation characterized by continuous uninterrupted firing in this specific region of the phase space. Our data then suggest that grid grouping is more robust against a transition to such a hyperactive state.

Adding inhibitory neurons has the effect of decreasing the degree of synchronization, as seen by others [33]. This addition also reduces the difference between the grouped and mixed networks, an effect that can be attributed to the inhibitory neurons connecting neurons across groups, thus decreasing the effect of spatial groupings, and also preventing the mixed system from a state of continuous activity.

We find an interesting and complementary conclusion when considering the larger region of the phase diagram where there is practically no difference in the firing dynamics of the two groups [blue regions in Fig. 7(a)]. Our results indicate that this similarity in dynamics exists even when

the two groups are wired in totally different ways leading to different average connection lengths (see Figs. S9 and S10) and signal distances. These results suggests that, for these regions of the phase diagram, there is a disconnection between topology and function as defined by the SPIKE-distance measure. This nondependent behavior is akin to the observation that orientational columns in the ocular cortex of the monkey do not talk to each other while ocular dominance columns do in the same region of space pointing to some independence of morphology and function [54,55].

Nonetheless, this complementary conclusion does not rule out a relationship between topology and synchronization as shown by our data. First, in the region of high connections per neuron in the grid grouping, the SPIKE distance is proportional to the average signal distance. This suggests that shorter average connections and signal paths between neurons do play a role in making the networks more synchronous. This is consistent with the concept of economies of connection [56,57] that may be playing a role. Second, the area where synchronization differs is still one where signal distances [Fig. 8(a)] and average connection lengths (Fig. S9) differ, with the grid grouping having lower values for both, in contrast to the thought that highly clustered networks have a higher connection cost than a random network [3]. This region is one with high δ, which forms a sparse intergroup connection scheme with shorter connections lengths where the economy of connections may be at work. It is not hard to imagine that given a network with the connection constraints given by this region of phase space, biological systems faced with the cost of wiring but with the same topological integration could in fact choose to use the grid grouping rather than the mixed one [3,58].

Many elements of our model are not new. Many studies explore clustering and small-world connectivity in the context of neuronal network simulations [22,32,33,59]. However, the number of studies on the effects of the overlap between clustering and distance-dependent time delays is rather small [32]. There are in some cases differences in the results between these previous studies and ours. For example, in a 2D all-connected network researchers find that signal time delays always disrupt synchronization [31], while we find that by increasing intergroup connectivity, an asynchronous to synchronous transition always occurs despite the existence of a delay in the signal. In other cases, our results are consistent with others, such as in a study considering distance-dependent delays with neurons scattered in a 3D cube and with connections tunable between scale-free and nearest-neighbor connections [32]. This study finds that the most synchronized network is the one intermediary between both connectivity regimes. Because their connectivities do not spatially separate their connected groups, their connectivity model is more akin to our mixed grouping, in which we also find an optimum degree of synchronization at a rather high value of intergroup connectivity (mid–low δ). Without time delays, it is understood analytically that synchronization within groups can enhance the synchronizability of the network [60] and that high intergroup connectivity can lead to this condition being met [61], but work like ours and that of Gosak [32] show that with the introduction of distance-dependent time delays, this effect is not universal and is only met within a certain range of connectivity conditions due to the high variability of delay times.

Our model can be modified to improve some of its simplifying assumptions, such as the construction of connections following a random process. It is known that connectivity in the brain is not random, and that motifs (two- and three-neuron) of highly connected neurons are overrepresented [12]. Although considering such connectivity might introduce changes to our phase diagrams, we do not expect that our main conclusions would change because our results are based on the difference between two neuronal groupings that could in principle cancel individual changes. Nonetheless, a future consideration of our modeling will test whether inclusion of such a connectivity might introduce significant changes.

V. CONCLUSIONS

Our results show that a computational model of neuronal networks with distance-dependent time delays can exhibit a high degree of spiking synchrony throughout the network when enough connections are formed between neurons, but that this can be lost if the network enters a hyperactive state characterized by continuous firing of excitatory neurons. This state appears in networks with relatively isolated groups (high δ) that are spatially mixed, but it does not appear when these same groups are spatially segregated into a grid (columnar) structure. The robustness of the grid networks is understood in terms of properties of the distances between neurons while the hyperactive state is understood by the group dynamics of firing neurons. Further investigation is needed to isolate factors that lead to the transition to this hyperactive state, but from the presented data it is clear that networks with grid grouping are more robust against transitioning into this continuous activity state.

ACKNOWLEDGMENT

Thanks to Lindsay Leverett for editing contributions.

[1] O. Sporns and J. D. Zwi, The small world of the cerebral cortex, Neuroinformatics **2**, 145 (2004).

[2] D. S. Bassettt, A. Meyer-Lindenberg, S. Achard, T. Duke, and E. T. Bullmore, Adaptive reconfiguration of fractal small-world human brain functional networks, Proc. Nat. Acad. Sci. USA **103**, 19518 (2006).

[3] E. T. Bullmore and O. Sporns, Complex brain networks: Graph theoretical analysis of structural and functional systems, Nature Rev. Neurosci. **10**, 186 (2009).

[4] G. L. Gong, Y. He, L. Concha, C. Lebel, D. W. Gross, A. C. Evans, and C. Beaulieu, Mapping anatomical connectivity patterns of human cerebral cortex using in vivo

diffusion tensor imaging tractography, Cereb. Cortex **19**, 524 (2009).

[5] D. Meunier, R. Lambiotte, and E. T. Bullmore, Modular and hierarchically modular organization of brain networks, Front. Neurosci. **4**, 200 (2010).

[6] D. S. Bassett, D. L. Greenfield, A. Meyer-Lindenberg, D. R. Weinberger, S. W. Moore, and E. T. Bullmore, Efficient physical embedding of topologically complex information processing networks in brains and computer circuits, PLoS Comput. Biol. **6**, e1000748 (2010).

[7] C. J. Stam, B. F. Jones, G. Nolte, M. Breakspear, and Ph. Scheltens, Small-world networks and functional connectivity in alzheimer's disease, Cereb. Cortex **17**, 92 (2007).

[8] W. de Haan, Y. A. L. Pijnenburg, R. L. M. Strijers, Y. van der Made, W. M. van der Flier, P. Scheltens, and C. J. Stam, Functional neural network analysis in frontotemporal dementia and alzheimer's disease using eeg and graph theory, BMC Neuroscience **10** (2009).

[9] M. Rubinov, S. A. Knock, C. J. Stam, S. Micheloyannis, A. W. F. Harris, L. M. Williams, and M. Breakspear, Small-world properties of nonlinear brain activity in schizophrenia, Human Brain Mapping **30**, 403 (2009).

[10] H. Markram, J. Lubke, M. Frotscher, A. Roth, and B. Sakmann, Physiology and anatomy of synaptic connections between thick tufted pyramidal neurones in the developing rat neocortex, J. Physiol. London **500**, 409 (1997).

[11] A. M. Thomson and A. P. Bannister, Interlaminar connections in the neocortex, Cereb. Cortex **13**, 5 (2003).

[12] S. Song, P. J. Sjöström, M. Reigl, S. Nelson, and D. B. Chklovskii, Highly nonrandom features of synaptic connectivity in local cortical circuits, PLoS Biol. **3**, e68 (2005).

[13] R. F. Betzel and D. S. Bassett, Multi-scale brain networks, Neuroimage, **160**, 73 (2017).

[14] H. Ko, S. B. Hofer, B. Pichler, K. A. Buchanan, P. J. Sjostrom, and T. D. Mrsic-Flogel, Functional specificity of local synaptic connections in neocortical networks, Nature (London) **473**, 87 (2011).

[15] R. Perin, T. K. Berger, and H. Markram, A synaptic organizing principle for cortical neuronal groups, Proc. Nat. Acad. Sci. USA **108**, 5419 (2011).

[16] R. Perin, M. Telefont, and H. Markram, Computing the size and number of neuronal clusters in local circuits, Front. Neuroanat. **7** (2013), doi:10.3389/fnana.2013.00001.

[17] J. H. Downes, M. W. Hammond, D. Xydas, M. C. Spencer, V. M. Becerra, K. Warwick, B. J. Whalley, and S. J. Nasuto, Emergence of a small-world functional network in cultured neurons, PLoS Comput. Biol. **8**, e1002522 (2012).

[18] G. Zamora-Lopez, C. S. Zhou, and J. Kurths, Graph analysis of cortical networks reveals complex anatomical communication substrate, Chaos **19**, 015117 (2009).

[19] G. Zamora-Lopez, C. S. Zhou, and J. Kurths, Exploring brain function from anatomical connectivity, Front. Neurosci. **5**, 11 (2011).

[20] S.-J. Wang, C. C. Hilgetag, and C. Zhou, Sustained activity in hierarchical modular neural networks: self-organized criticality and oscillations, Front. Comput. Neurosci. **5**, 30 (2011).

[21] M. Zhao, C. S. Zhou, J. H. Lü, and C. H. Lai, Competition between intra-community and inter-community synchronization and relevance in brain cortical networks, Phys. Rev. E **84**, 016109 (2011).

[22] C. A. S. Batista, E. L. Lameu, A. M. Batista, S. R. Lopes, T. Pereira, G. Zamora-López, J. Kurths, and R. L. Viana, Phase synchronization of bursting neurons in clustered small-world networks, Phys. Rev. E **86**, 016211 (2012).

[23] M. Vegue, R. Perin, and A. Roxin, On the structure of cortical microcircuits inferred from small sample sizes, J. Neurosci. **37**, 8498 (2017).

[24] O. Sporns and R. F. Betzel, Modular brain networks, Annu. Rev. Physiol. **67**, 613 (2016).

[25] M. Shimono and J. M. Beggs, Functional clusters, hubs, and communities in the cortical microconnectome, Cereb. Cortex **25**, 3743 (2015).

[26] A. Nematzadeh, E. Ferrara, A. Flammini, and Y.-Y. Ahn, Optimal Network Modularity for Information Diffusion, Phys. Rev. Lett. **113**, 088701 (2014).

[27] G. L. Baum, R. Ciric, D. R. Roalf, R. F. Betzel, T. M. Moore, R. T. Shinohara, A. E. Kahn, S. N. Vandekar, P. E. Rupert, M. Quarmley, P. A. Cook, M. A. Elliott, K. Ruparel, R. E. Gur, R. C. Gur, D. S. Bassett, and T. D. Satterthwaite, Modular segregation of structural brain networks supports the development of executive function in youth, Curr. Biol. **27**, 1561 (2017).

[28] D. Guo, Q. Wang, and M. Perc, Complex synchronous behavior in interneuronal networks with delayed inhibitory and fast electrical synapses, Phys. Rev. E **85**, 061905 (2012).

[29] K. M. Kutchko and F. Fröhlich, Emergence of metastable state dynamics in interconnected cortical networks with propagation delays, PLoS Comput. Biol. **9**, e1003304 (2013).

[30] X. Sun and G. Li, Synchronization transitions induced by partial time delay in a excitatory-inhibitory coupled neuronal network, Nonlinear Dynamics **89**, 2509 (2017).

[31] G. Tang, K. Xu, and L. Jiang, Synchronization in a chaotic neural network with time delay depending on the spatial distance between neurons, Phys. Rev. E **84**, 046207 (2011).

[32] M. Gosak, R. Markovic, and M. Marhl, The role of neural architecture and the speed of signal propagation in the process of synchronization of bursting neurons, Physica A **391**, 2764 (2012).

[33] H. Li, X. Sun, and J. Xiao, Degree of synchronization modulated by inhibitory neurons in clustered excitatory-inhibitory recurrent networks, Europhys. Lett. **121**, 10003 (2018).

[34] Y. J. Wang and G. Y. Wong, Stochastic blockmodels for directed graphs, J. Am. Stat. Assoc. **82**, 8 (1987).

[35] P. N. Steinmetz, A. Roy, P. J. Fitzgerald, S. S. Hsiao, K. O. Johnson, and E. Niebur, Attention modulates synchronized neuronal firing in primate somatosensory cortex, Nature (London) **404**, 187 (2000).

[36] P. Fries, J. H. Reynolds, A. E. Rorie, and R. Desimone, Modulation of oscillatory neuronal synchronization by selective visual attention, Science **291**, 1560 (2001).

[37] A. Buehlmann and G. Deco, Optimal information transfer in the cortex through synchronization, PLoS Comput. Biol. **6**, e1000934 (2010).

[38] L. G. Dominguez, R. A. Wennberg, W. Gaetz, D. Cheyne, O. Carter Snead, and J. L. P. Velazquez, Enhanced synchrony in epileptiform activity? local versus distant phase synchronization in generalized seizures, J. Neurosci. **25**, 8077 (2005).

[39] See Supplemental Material at http://link.aps.org/supplemental/10.1103/PhysRevE.101.022408 for neuron simulation parameters and further analysis referenced in the main text.

[40] A. M. Packer and R. Yuste, Dense, unspecific connectivity of neocortical parvalbumin-positive interneurons: A canonical microcircuit for inhibition? J. Neurosci. **31**, 13260 (2011).
[41] D. J. Watts and S. H. Strogatz, Collective dynamics of 'small-world' networks, Nature (London) **393**, 440 (1998).
[42] N. T. Carnevale and M. L. Hines, *The NEURON Book* (Cambridge University Press, Cambridge, 2006).
[43] A. Destexhe, D. Contreras, and M. Steriade, Mechanisms underlying the synchronizing action of corticothalamic feedback through inhibition of thalamic relay cells, J. Neurophysiol. **79**, 999 (1998).
[44] D. A. McCormick, Z. Wang, and J. Huguenard, Neurotransmitter control of neocortical neuronal activity and excitability, Cereb. Cortex **3**, 387 (1993).
[45] L. Cruz, B. Urbanc, A. Inglis, D. L. Rosene, and H. E. Stanley, Generating a model of the three-dimensional spatial distribution of neurons using density maps, Neuroimage **40**, 1105 (2008).
[46] J. D. Victor and K. P. Purpura, Nature and precision of temporal coding in visual cortex: A metric-space analysis, J. Neurophysiol. **76**, 1310 (1996).
[47] J. D. Victor and K. P. Purpura, Metric-space analysis of spike trains: Theory, algorithms and application, Netw., Comput. Neural Syst. **8**, 127 (1997).
[48] M. C. W. van Rossum, A novel spike distance, Neural Comput. **13**, 751 (2001).
[49] T. Kreuz, D. Chicharro, M. Greschner, and R. G. Andrzejak, Time-resolved and time-scale adaptive measures of spike train synchrony, J. Neurosci. Methods **195**, 92 (2011).
[50] T. Kreuz, D. Chicharro, C. Houghton, R. G. Andrzejak, and F. Mormann, Monitoring spike train synchrony, J. Neurophysiol. **109**, 1457 (2013).
[51] F. Lombardi, H. J. Herrmann, and L. de Arcangelis, Balance of excitation and inhibition determines 1/f power spectrum in neuronal networks, Chaos **27**, 047402 (2017).
[52] T. P. Peixoto, The graph-tool python library, figshare, (2014).
[53] M. P. van den Heuvel, E. T. Bullmore, and O. Sporns, Comparative connectomics, Trends Cognit. Sci. **20**, 345 (2016).
[54] D. H. Hubel and T. N. Wiesel, Uniformity of monkey striate cortex: A parallel relationship between field size, scatter, and magnification factor, J. Comp. Neurol. **158**, 295 (1974).
[55] N. Macarico da Costa and K. A. C. Martin, Whose cortical column would that be? Front. Neuroanatomy **4**, 16 (2010).
[56] D. H. Hubel and T. N. Wiesel, Receptive fields, binocular interaction and functional architecture in the cat's visual cortex, J. Physiol. **160**, 106 (1962).
[57] D. H. Hubel and T. N. Wiesel, Sequence regularity and geometry of orientation columns in the monkey striate cortex, J. Comp. Neurol. **158**, 267 (1974).
[58] M. Schroter, O. Paulsen, and E. T. Bullmore, Micro-connectomics: probing the organization of neuronal networks at the cellular scale, Nature Rev. Neurosci. **18**, 131 (2017).
[59] T. de L. Prado, S. R. Lopes, C. A. S. Batista, J. Kurths, and R. L. Viana, Synchronization of bursting hodgkin-huxley-type neurons in clustered networks, Phys. Rev. E **90**, 032818 (2014).
[60] F. Sorrentino and E. Ott, Network synchronization of groups, Phys. Rev. E **76**, 056114 (2007).
[61] J. Stroud, M. Barahona, and T. Pereira, *Dynamics of Cluster Synchronisation in Modular Networks: Implications for Structural and Functional Networks* (Springer, Berlin, 2015), Vol. 4, pp 107–130.